arXiv:1302.3504v1 [cond-mat.quant-gas] 14 Feb 2013

Superconducting Vortex Lattices for Ultracold Atoms

O. Romero-Isart[1], C. Navau[2], A. Sanchez[2], P. Zoller[3,4], and J. I. Cirac[1]
[1] *Max-Planck-Institut für Quantenoptik, Hans-Kopfermann-Strasse 1, D-85748, Garching, Germany.*
[2] *Grup d'Electromagnetisme, Departament de Física,*
Universitat Autònoma de Barcelona, 08193 Bellaterra, Barcelona, Catalonia, Spain.
[3] *Institute for Theoretical Physics, University of Innsbruck, A-6020 Innsbruck, Austria. and*
[4] *Institute for Quantum Optics and Quantum Information of the Austrian Academy of Sciences, A-6020 Innsbruck, Austria.*

The ability to trap and manipulate ultracold atoms in lattice structures has lead to a remarkable experimental progress to build quantum simulators for Hubbard models. A prominent example is atoms in optical lattices where lasers are used to create lattices with spacing set by the laser wavelength as well as to control and measure the many-body states. In contrast, here we propose and analyze a nanoengineered vortex array in a thin-film type-II superconductor as a magnetic lattice for ultracold atoms. This proposal addresses several of the key questions in the development of atomic quantum simulators. By trapping atoms close to the surface, tools of nanofabrication and structuring of lattices on the scale of few tens of nanometers become available with a corresponding benefit in energy scales and temperature requirements. This can be combined with the possibility of magnetic single site addressing and manipulation together with a favorable scaling of superconducting surface induced decoherence.

Optical lattices allow to confine ultracold neutral atoms in highly controllable periodic potentials designed by the interference pattern of counterpropagating lasers [1, 2]. This possibility has triggered several research fields during the last decade, in particular, quantum simulation of many-body physics [3, 4], quantum computation [5], and quantum metrology [6]. Remarkably, the quantum simulation of Bose- and Fermi-Hubbard hamiltonians holds the promise to be the first technology that can solve problems not accessible to classical computers [7]. An important challenge to achieve this goal is the development of better cooling schemes in order to reduce the entropy of the simulator [3]. Effectively, this could be achieved by boosting the energy scale of the physical parameters of the quantum simulator by scaling down the lattice potential, namely by reducing the distance between lattice sites. Due to the diffraction limit, this requires to trap atoms near a surface without adding new sources of decoherence, which results in a challenging trade-off, see for instance the recent proposal based on nanoplasmonic optical lattices [8]. However, placing atoms close to surfaces also makes available the tools of nanofabrication to engineer arbitrary (periodic and non-periodic) atomic lattice structures.

Here, we propose and analyze a new approach to trap and manipulate ultracold neutral atoms in arbitrary lattice potentials based on using a magnetic nanolattice generated by a controlled array of superconducting vortices in thin films. While magnetic traps for ultracold atoms created by macroscopic currents flowing in type-II superconducting materials (the ones that contain vortices) have been theoretically proposed and experimentally realized [9–14], here, we aim at something radically different and more challenging, namely to trap single atoms using the field created by few controlled superconducting vortices. That is, we propose to exploit the nanoscience and technology developed to manipulate superconducting vortices in thin films [15] for atomic physics. This technology has the goal of controlling the electronic properties of superconducting devices that are strongly affected by the presence and motion of vortices. In particular, today superconducting vortices can be positioned more or less at wish, even in complex structures, by artificially pinning them in nanoengineered arrays of, for instance, completely etched holes (antidots) of various sizes and shapes, see [15] and references therein. Our proposal hints at the possibility to fabricate and structure magnetic lattices at the fundamental length scales associated to superconducting vortices, which can be of few tens of nanometers, and hence render magnetic lattices to an unprecedented hitherto parameter regime [16–19]. Moreover, the combination of all-magnetic trapping and manipulation and superconducting surfaces leads, in principle, to very favorable scalings on surface-induced decoherence, as discussed below.

Superconducting Vortex Lattice

We consider a superconducting film of thickness $d \lesssim \lambda$, where λ is the London penetration depth. The film is a type-II superconductor, *i.e.*, $\lambda/\xi > 1/\sqrt{2}$, where ξ is the coherence length whose value is typically between few to tens of nanometers [20]. In thin films, the effective penetration depth is given by $\Lambda = \lambda^2/d \gtrsim \lambda \gtrsim d > \xi$, which hence can potentially be as small as few tens of nanometers. The upper side of the film is situated at the $x-y$ plane with $z=0$ and contains a periodic array of superconducting vortices distributed in a Bravais lattice $\mathbf{R} = n_1\mathbf{a}_1 + n_2\mathbf{a}_2$, where $\mathbf{a}_{1(2)}$ are the lattice primitive vectors and $n_{1(2)}$ range through all integer values. The density of vortices is $1/a^2$ where $a^2 = |\mathbf{a}_1 \times \mathbf{a}_2|$ is the area of the primitive cell. Each vortex creates a

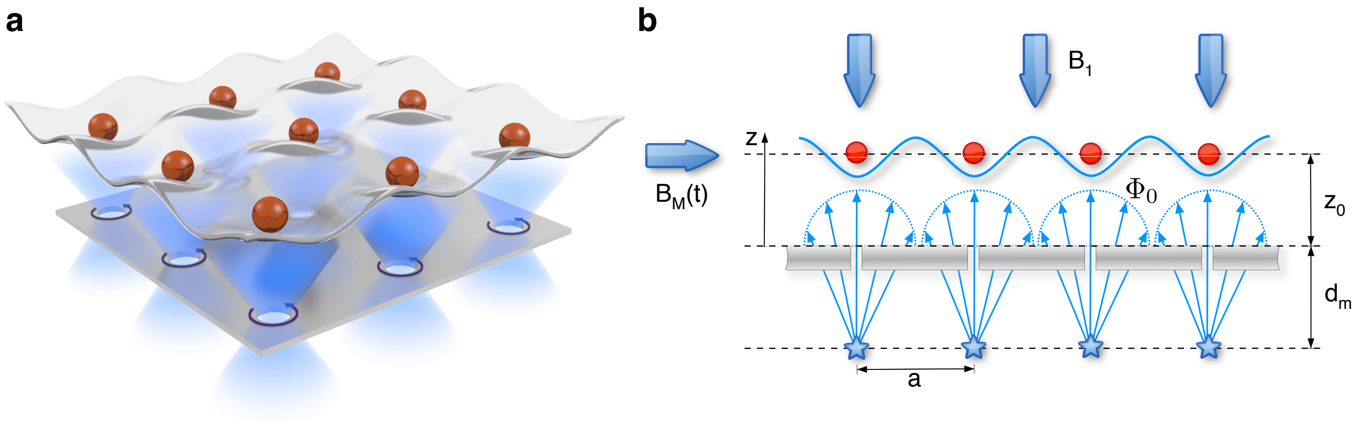

FIG. 1: **Superconducting vortex nanolattice**. a) An array of completely-etched holes (antidots) with a commensurate number of vortices creates a magnetic field that can be used to trap neutral atoms in a two-dimensional magnetic lattice with the same lattice geometry as the vortex lattice. b) The distance between vortices is given by a and atoms are trapped at a distance z_0 from the upper side of the film. The magnetic field generated by a vortex can be approximated by the field generated by a monopole situated at $z = -d_{\mathrm{m}} \sim \Lambda$ of charge $2\Phi_0$. The trapping along the z-axis is achieved by applying a perpendicular and homogeneous magnetic field of strength B_1. A time-dependent bias field parallel to the film $\mathbf{B}_{\mathrm{M}}(t)$ is applied to create a time-averaged orbiting potential which is employed to circumvent Majorana losses.

magnetic flux given by $\Phi_0 = h/(2e)$, where $h = 2\pi\hbar$ is Planck's constant and e the charge of the electron. In superconducting films with a low intrinsic pinning, a triangular lattice minimizes the vortex-vortex repulsive interaction [20]. In this case, the maximum vortex density is limited to $1/\xi^2$, which corresponds to the situation when the cores of the vortices overlap. Other lattice geometries can be considered by nanoengineering a periodic array of artificial pinning centers consisting of antidots of radius $R \gtrsim \xi$ [15]. The artificial pinning sites attract the vortices very strongly [21, 22] and, as a result, the underlying symmetry of the pinning array dictates the symmetry of stable vortex patterns. The interplay between the interaction of vortices with the pinning lattice and the vortex-vortex repulsion leads to interesting phase diagrams for the crystallization of vortices [27]. In the following, we assume that the vortices stabilize at the pinning lattice if the density of antidots does not exceed $1/a^2 \lesssim 1/\Lambda^2$, see Supplemental Information (SI) for further discussion. The vortex lattice can be prepared by cooling the film in the presence of an homogeneous perpendicular matching field of strength $B_{\mathrm{a}} = \Phi_0/a^2$ such that a commensurate number of superconducting vortices is created in the antidot lattice. At the final temperature below T_{c} (which can be of a high-T_{c} material) the applied field is switched-off and the vortices remain.

Magnetic field generated by the vortex lattice

Our proposal consists in using the magnetic field created by the vortex lattice above the film $\mathbf{B}_{\mathrm{V}}(\mathbf{r}, z > 0)$ to trap neutral atoms in a two-dimensional magnetic nanolattice with a geometry dictated by the nanoengineered antidot lattice, see Fig 1a. Hence, we need to calculate $\mathbf{B}_{\mathrm{V}}(\mathbf{r}, z > 0)$, which for an infinite arbitrary array of superconducting vortices is a complicated task. For a triangular lattice, this has been discussed within the Ginzburg-Landau theory [23], but its expression is cumbersome. In the following, we will make use of a simplified model that allows us to obtain $\mathbf{B}_{\mathrm{V}}(\mathbf{r}, z > 0)$ very accurately with a simple expression. First, we consider the London limit $\lambda \gg \xi$, such that the currents and field generated by a vortex in a thin film can be analytically obtained [24], see SI. Furthermore, as discussed in [25, 26] and in the SI, the field above the film created by a single vortex situated at $\mathbf{R}$, which we denote by $\mathbf{B}_{\mathbf{R}}(\mathbf{r}, z > 0)$, can be very well approximated by the one created by a magnetic monopole situated at $z = -d_{\mathrm{m}} \sim -\Lambda$ and with a charge $2\Phi_0$ such that a flux Φ_0 passes through the semicircle of radius $[|\mathbf{r}-\mathbf{R}|^2 + (z+d_{\mathrm{m}})^2]^{1/2}$. That is, we will use

$$\mathbf{B}_{\mathbf{R}}(\mathbf{r}, z > 0) \approx \frac{\Phi_0}{2\pi} \frac{(\mathbf{r}-\mathbf{R}, z+d_{\mathrm{m}})}{[|\mathbf{r}-\mathbf{R}|^2 + (z+d_{\mathrm{m}})^2]^{3/2}}. \tag{1}$$

Using this approximation, see Fig. 1b, we can calculate the field $\mathbf{B}_{\mathrm{V}}$ generated by an arbitrary vortex lattice $\{\mathbf{R}\}$ by solving the Poisson equation $\nabla^2\phi(\mathbf{r}, z) = -\rho(\mathbf{r}, z)$, where $\mathbf{B}_{\mathrm{V}}(\mathbf{r}, z) = -\nabla\phi(\mathbf{r}, z)$, $\rho(\mathbf{r}, z) = 2\Phi_0\delta\left(z + d_{\mathrm{m}}\right)\sum_{\mathbf{R}}\delta\left(\mathbf{r}-\mathbf{R}\right)$, and $\delta()$ is the Dirac delta function. This can be analytically solved by Fourier transformation into the reciprocal space, where in this case $\rho(\mathbf{r}, z) = 2B_0\delta\left(z + d_{\mathrm{m}}\right)\sum_{\mathbf{K}} e^{-\mathrm{i}\mathbf{K}\cdot\mathbf{r}}$. The sum is over all reciprocal lattice vectors $\mathbf{K}$ and we have defined $B_0 \equiv \Phi_0/a^2$. As shown in the SI, the solution of the

Poisson equation leads to

$$\begin{aligned} B_{\mathrm{V}}^{x(y)}(\mathbf{r},z) &= B_0 e^{-\Delta_z} g_{x(y)}(\mathbf{r},z), \\ B_{\mathrm{V}}^{z}(\mathbf{r},z) &= B_0 \left[1 + e^{-\Delta_z} g_z(\mathbf{r},z)\right], \end{aligned} \tag{2}$$

where we have defined $\Delta_z \equiv 2k(z+d_{\mathrm{m}}) > 2kd_{\mathrm{m}} \equiv \Delta_{\mathrm{min}}$, $k \equiv \pi/a$, and,

$$\begin{aligned} g_{x(y)}(\mathbf{r},z>0) &\equiv \sum_{\mathbf{K}\neq\mathbf{0}} \frac{K_{x(y)}}{|\mathbf{K}|} \sin(\mathbf{K}\cdot\mathbf{r}) e^{\Delta_z(1-|\mathbf{K}|/k)}, \\ g_z(\mathbf{r},z>0) &\equiv \sum_{\mathbf{K}\neq\mathbf{0}} \cos(\mathbf{K}\cdot\mathbf{r}) e^{\Delta_z(1-|\mathbf{K}|/k)}. \end{aligned} \tag{3}$$

The x and y components of $\mathbf{B}_{\mathrm{V}}$ are equal zero on top of the vortices, namely at $\mathbf{r} = \mathbf{R}$. The z component is always positive and tends to an homogeneous field of strength B_0 at long distance from the surface. The non-zero value of the field at long distances is a consequence of the infinite extension of the plane. Note that general non-periodic structures obtained by nanoengineering can also be considered.

Magnetic lattice potential for ultracold atoms

Alkali metal atoms in low fields of strength $\lesssim$ 30 mT, where the Zeeman shift of hyperfine levels is linear, experience a potential of the form $V_{\mathrm{lat}}(\mathbf{r},z) = \mu_{m_F}|\mathbf{B}(\mathbf{r},z)|$ [28, 29]. The local field interacting with the atoms is denoted by $\mathbf{B}$ and will be composed by the one generated by the vortices $\mathbf{B}_{\mathrm{V}}$ plus additional bias fields, see below. The magnetic dipole moment is given by $\mu_{m_F} \equiv m_F g_F \mu_{\mathrm{B}}$, where m_F is the magnetic quantum number, g_F is the Landé g-factor, and the positive number μ_{B} is the Bohr magneton. Thus, low-field-seeker states $g_F m_F > 0$ can be trapped at the local minima of $|\mathbf{B}(\mathbf{r},z)|$ [28, 29]. The form of the potential assumes that the projection of the atomic magnetic moment into the instantaneous direction of magnetic field is constant, an assumption that we take into account below.

The field generated by the vortices does not have local minima of $|\mathbf{B}_{\mathrm{V}}|$ since as discussed in the previous section, the z-component is always positive. For this reason, we propose to add a perpendicular bias field of the form $\mathbf{B}_1 = B_1(0,0,-1)$ and define $\mathbf{B}_{\mathrm{lat}}(\mathbf{r},z) = \mathbf{B}_{\mathrm{V}}(\mathbf{r},z) + \mathbf{B}_1$. The field $\mathbf{B}_1$ can be considered homogeneous even close to the surface provided that a thin film of $d \lesssim \lambda$ is used. We have validated this assumption by numerically calculating the field distribution and induced currents in a superconducting disk of finite radius and thickness using an energy minimization procedure [30] taking into account their kinetic and magnetic energy terms [31], see SI. The strength of B_1 is limited by the fact that it should not induce vortices in the central region of the film. This leads to the condition $B_1 < B^\star + \min_{\mathbf{r}} B_{\mathrm{V}}^z(\mathbf{r},0)$, where $B^\star \approx \Phi_0/(4\pi\Lambda^2)$. The local minima of $|\mathbf{B}_{\mathrm{lat}}(\mathbf{r},z)|$ are obtained on top of the vortices, $\mathbf{r} = \mathbf{R}$, when $B_1 > B_0$, at a position z_0 given by the solution of the equation $B_{\mathrm{V}}^z(\mathbf{R},z_0) = B_1$, see Fig. 2a, where we have defined $\Delta \equiv \Delta_{z_0}$. In this case, the conditions $B^\star > B_1 > B_0$ can be fulfilled provided $\Lambda \gtrsim a$. In Fig. 3 we plot $|\mathbf{B}_{\mathrm{lat}}|^2$ (as the final form the potential depends on the modulus square, see Eq. (4)) in the $x-z$ plane (at $y=0$). As a validation of the model, we plot the same quantity for an array of 3×3 vortices in a finite plane numerically solving the London equation using the method presented in [32]. One can observe that there is also a minimum of $|\mathbf{B}_{\mathrm{lat}}(\mathbf{r},z)|^2$ on top of the central vortex. In the case $B_1 < B_0$, one confines atoms between vortices with a much shallower trap, see Fig. 2a.

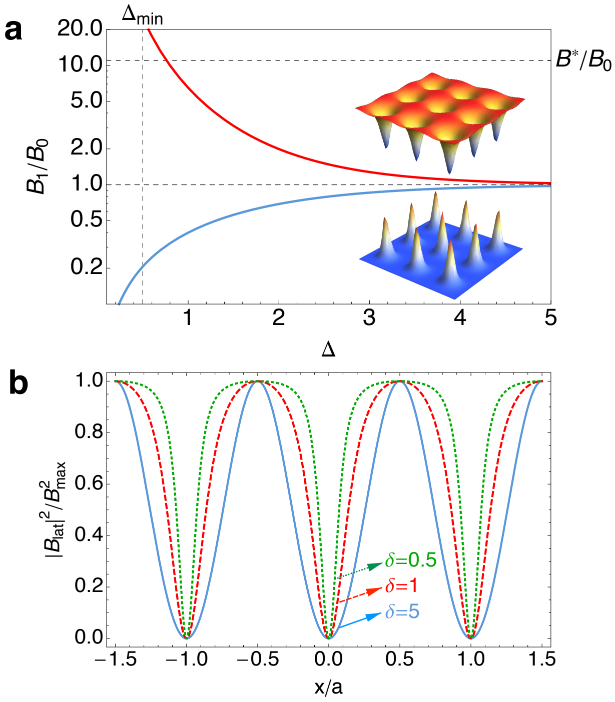

FIG. 2: **Lattice control with the perpendicular bias field**. a) Relation between the applied field B_1 and the dimensionless parameter $\Delta = 2\pi(z_0+d_{\mathrm{m}})/a$. Since z_0 can only be positive, Δ has a minimum given by $\Delta_{\mathrm{min}} = 2\pi d_{\mathrm{m}}/a$. B_1 is also upper-limited by the field $B^\star$ in order not to induce vortices. At $B_1 = 0$ there is no confinement along the z-axis. In the inset we plot $|\mathbf{B}_{\mathrm{lat}}(x,y,z_0)|^2$ for a square lattice and $\Delta = 2$ for $B_1 > B_0$ (deep wells) and $B_1 < B_0$ (sharp peaks). b) $|\mathbf{B}_{\mathrm{lat}}|^2$ as a function of x/a at $y=0$ and $z=z_0$ for a square lattice for different Δ. $|\mathbf{B}_{\mathrm{lat}}|^2$ is plotted in units of $B^2_{\mathrm{max}} \equiv |\mathbf{B}_{\mathrm{lat}}(x=a/2,0,z_0)|^2$. As seen in the plot, the smaller the Δ, the more Fourier components are involved in $|\mathbf{B}_{\mathrm{lat}}|^2$ as a function of x.

It is well known that Majorana losses [33], namely spontaneous spin flips rendering the state of the atom into a high-field-seeker, occur when $|\mathbf{B}| \sim 0$. Note that the minima of $|\mathbf{B}_{\mathrm{lat}}|$ correspond to zero-field. In order

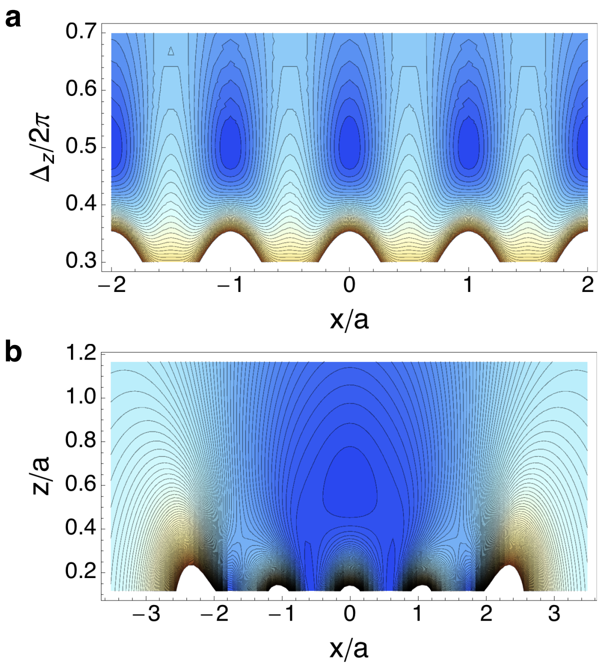

FIG. 3: **Magnetic field distribution**. a) A contour plot of $|\mathbf{B}_{\rm lat}|^2$ at $y = 0$ is shown for a square lattice as a function of x/a and $\Delta_z = 2\pi(z+d_{\rm m})/a$ for $\Delta = 2\pi(z_0+d_{\rm m})/a = \pi$. This is done using Eq. (2), which is calculated using the approximation of the monopoles and for an infinite lattice. The local minima $|\mathbf{B}_{\rm lat}|^2$ on top of the vortices are clearly observed. b) The same plot as a) is done with a set of 3x3 localized vortices located on a squared lattice in a thin superconductor. $|\mathbf{B}_{\rm lat}|^2$ is calculated by numerically solving the London equation using the method presented in [32] and using $\Lambda \approx a$. A local minimum is also observed on top of the central vortex. Note also the boundary effects (the borders of the plane are at $x/a = \pm 2.45$.

to prevent Majorana losses we suggest to use an effective time-averaged, orbiting potential [34] generated by adding to $\mathbf{B}_{\rm lat}$ an homogeneous time-dependent field parallel to the thin film $\mathbf{B}_{\rm M}(t) = B_{\rm M}(\sin\omega_{\rm M}t, \cos\omega_{\rm M}t, 0)$. By time-averaging we have that $\langle \mathbf{B}_{\rm M}(t)\rangle = \mathbf{0}$, but $\langle|\mathbf{B}_{\rm M}(t)|\rangle = B_{\rm M}$. Assuming $B_{\rm M} \gg \max|\mathbf{B}_{\rm lat}(\mathbf{r}, z_0)|$ and considering that the total field experienced by the atoms is given by $\mathbf{B} = \mathbf{B}_{\rm lat} + \mathbf{B}_{\rm M}$, we have $\langle|\mathbf{B}|\rangle \approx B_M + |\mathbf{B}_{\rm lat}|^2/(2B_{\rm M})$, which does not contain zero-field local minima. Using that the oscillation frequency of the atom $\omega_{\rm t}$ is much smaller than $\omega_{\rm M}$, and $\omega_{\rm M}$ much smaller than the Larmor frequency (so that the atomic potential depends on the modulus of the magnetic field), namely $\omega_{\rm t} \ll \omega_{\rm M} \ll \omega_{\rm L} \equiv \mu_{m_F} B_{\rm M}/\hbar$, the effective time-averaged magnetic potential for the atoms is given by [34]

$$V_{\rm lat}(\mathbf{r}, z) \approx \hbar\omega_{\rm L} + \frac{\mu_{m_F}}{2B_{\rm M}}|\mathbf{B}_{\rm lat}(\mathbf{r}, z)|^2. \qquad (4)$$

This potential depends on $|\mathbf{B}_{\rm lat}|^2$, avoids Majorana losses, and confines atoms on a magnetic lattice whose geometry is dictated by the vortex lattice. Note that the bias field B_1 can be used control the trapping position in the z-axis, see Fig. 2a. This might be used to adiabatically load the ultracold atoms into the magnetic lattice from an external trap.

Quantum simulation of Hubbard hamiltonians

A prominent application of the magnetic lattice potential Eq. (4) is the possibility to perform quantum simulation of quantum many-body physics. When loading an ultracold gas of neutral atoms into the magnetic lattice, atoms will be positioned at the local minima of the lattice potential. In this situation, atoms can tunnel to neighboring lattice sites and interact on-site due to short-ranged collisional interactions [2]. This leads to similar rich many-body physics encountered in typical condensed-matter physics, where electrons can be modeled as moving on a lattice generated by the periodic array of atom cores. The advantage of quantum simulators is the high-degree of controllability of purely conservative and defect-free lattice potentials. The hamiltonian describing the interaction of ultracold atoms in a lattice is given by a Hubbard model, which is one of the most paradigmatic models in condensed-matter physics [4]. For bosonic atoms, the Hubbard hamiltonian reads

$$\hat{H} = -t\sum_{\langle ij\rangle}\left(\hat{a}_i^\dagger\hat{a}_j + \hat{a}_j^\dagger\hat{a}_i\right) + U\sum_i \hat{n}_i\hat{n}_i, \qquad (5)$$

where $\hat{a}_i(\hat{a}_i^\dagger)$ annihilates (creates) a bosonic localized atom on site i, and $\hat{n}_i = \hat{a}_i^\dagger\hat{a}_i$. The first term describes tunneling between neighboring sites with tunnel coupling t, and the second on-site interactions with strength U. The particular interest of studying these type of models, in particular for spin=1/2 Fermionic atoms [35, 36], lies on the fact that in the strong coupling regime $U/t \gg 1$, superexchange processes provide the basic mechanism for an antiferromagnetic coupling between spins on neighbouring sites, which is closely related to studies of high-$T_{\rm c}$ superconductivity within the Hubbard model [37].

The strength of the Hubbard parameters and the dependence with the physical parameters of the superconducting vortex lattice (SVL) proposed here can be readily obtained in analogy to optical lattices (OLs) [1]. In particular, let us consider a square lattice with $B_1 > B_0$ and Δ sufficiently large, such that the potential Eq. (4) can be approximated to $V_{\rm lat}(\mathbf{r}, z) \approx V_0[\sin^2(kx) + \sin^2(ky)]$, where $V_0 \equiv 8B_0^2\exp[-2\Delta]\mu_{m_F}/B_{\rm M}$. This potential has the same form as the typical one obtained in OLs. The distance between the trapped atoms in the SVL is given by a, therefore $2a$ plays the role of the optical wavelength in OLs. The role of the laser intensity in OLs, that can be used to modulate the trap depth, is taken in the SVL by the strength of the bias field B_1, recall that Δ depends on B_1, see Fig. 2. Therefore, by defining $E_{\mathrm{R}} = \hbar^2 k^2/(2m_{\mathrm{a}})$, one can use the same formulas used in OLs to obtain the parameters in Hubbard hamiltonians [2, 35]: the trap frequency $\omega_{\mathrm{t}} \approx \sqrt{4E_{\mathrm{R}}V_0}/\hbar$, the tunneling rate $t \approx 2E_{\mathrm{R}}\left(V_0/E_{\mathrm{R}}\right)^{3/4}\exp\left[-2(V_0/E_{\mathrm{R}})^{1/2}\right]/\sqrt{\pi}$, and the on-site repulsion $U \approx \sqrt{8/\pi}E_{\mathrm{R}}a_{\mathrm{s}}k\left(V_0/E_{\mathrm{R}}\right)^{3/4}$, where a_{s} is the s-wave scattering length. In Fig. 4, we plot the tunneling rate as a function of a/Λ for Rb and Li (for $\Lambda = 100$ nm and $\Lambda = 20$ nm) and compare it with the decoherence rates that we discuss below. We also provide typical values for the trap frequencies in the caption of the figure. Since half the optical wavelength in some OLs can be of 250 nm [1], the case $\Lambda = 20$ nm supposes two orders of magnitude larger values of E_{R}, and therefore, significantly lower temperature requirements for the simulation of quantum magnetism in Hubbard hamiltonians [36].

The potential Eq. (4) also permits to design dense lattices with higher Fourier components, something that is very challenging to achieve in OLs. Here, by reducing Δ, more reciprocal vectors of different frequencies enter into play, see Fig. 2b. For $B_1 < B_0$ this can lead to interesting potentials with sharp repulsive structures, see the inset of Fig. 2a.

Decoherence due to thermal jiggling of vortices

Atoms in magnetic traps are subjected to decoherence due to magnetic field fluctuations at the Larmor frequency ω_{L}. These fluctuations yield spin-flips to untrapped atomic states, thereby leading to atom losses, as well as to motional heating [38]. In metal surfaces, these fluctuations are generated by thermally excited motion of electrons (Johnson Noise), as it is well understood in the context of atom chips [39]. Superconducting vortex-free surfaces have been predicted to dramatically reduce Johnson noise by 6-12 orders of magnitude [40–42]. However, experiments in superconducting atom chips have shown only a moderate improvement since they operate in a regime where uncontrolled superconducting vortices are present [43–46]. In the SVL proposed here, it is clear that a source of magnetic field fluctuations will be given by the thermal jiggling of the pinned vortices. In the SI we use a standard phenomenological model of vortex dynamics (see [48] and reference therein) in order to estimate the spin-flip rate Γ_{sf} and the motional heating rate $\Gamma_{0\to1}$ [38] induced by the thermal motion of vortices.

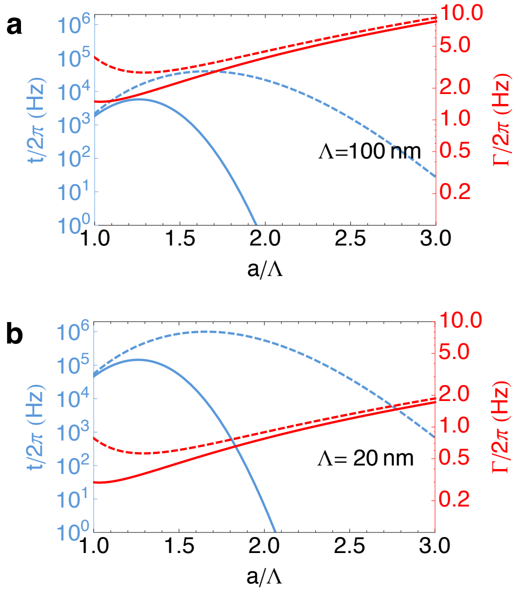

FIG. 4: **Tunneling vs. decoherence rates.** Tunneling rate t (left axis) for a square lattice at sufficiently large Δ such that the lattice potential can be approximated by $V_{\mathrm{lat}} = V_0(\sin^2 kx + \sin^2 ky)$, see text. This is plotted for Rubidium (solid lines) and Lithium (dashed line) for $\Lambda = 100$ nm, figure a), and for a more challenging value $\Lambda = 20$ nm, figure b). On the right axis the decoherence rate $\Gamma = \Gamma_{\mathrm{sf}} + \Gamma_{0\to1}$ due to thermal jiggling of vortices, see text, is plotted for Rubidium (solid line) and Lithium (dashed line). We have used $z_0 = d_m = \Lambda$ and chosen B_{M} such that $\omega_{\mathrm{L}} = 100\ \omega_{\mathrm{t}}$ (so that one can fulfill $\omega_{\mathrm{t}} \ll \omega_{\mathrm{d}} \ll \omega_{\mathrm{L}}$), which corresponds to fields up to ~ 1 mT (~ 10 mT) for $\Lambda = 100$ nm ($\Lambda = 20$ nm), $\mu_{m_F} = \mu_{\mathrm{B}}$ (Bohr's magneton), $\eta/\Lambda = 10^{-7}$ N/ms, and a temperature of $T = 4$ K. For $a = 1.5\ \Lambda$, one has that for $\Lambda = 100$ nm, $\omega_{\mathrm{t}}/2\pi \sim 9 \times 10^4$ Hz ($\sim 2 \times 10^5$ Hz) and $t/2\pi \sim 2 \times 10^3$ Hz ($\sim 3 \times 10^4$ Hz) for Rubidium (Lithium). Using $\Lambda = 20$ nm, then $\omega_{\mathrm{t}}/2\pi \sim 2 \times 10^6$ Hz ($\sim 5 \times 10^6$ Hz) and $t/2\pi \sim 5 \times 10^4$ Hz ($\sim 9 \times 10^5$ Hz).

They are given (up to some constant factors) by

$$\begin{aligned}\Gamma_{\mathrm{sf}} &\sim 3\pi^3\frac{\mu_{m_F}^2}{\hbar^2}\frac{k_{\mathrm{B}}T}{k_{\mathrm{p}}}\frac{\omega_{\mathrm{d}}}{\omega_{\mathrm{L}}^2+\omega_{\mathrm{d}}^2}\frac{B_0^2}{a^2\Delta^4},\\ \Gamma_{0\to1} &\sim (2\pi)^5\frac{\mu_{m_F}^2}{\hbar^2}\frac{k_{\mathrm{B}}T}{k_{\mathrm{p}}}\frac{\omega_{\mathrm{d}}}{\omega_{\mathrm{t}}^2+\omega_{\mathrm{d}}^2}\frac{x_0^2B_0^2}{a^4\Delta^6}.\end{aligned} \quad (6)$$

Here $x_0 = \sqrt{\hbar/(2m_{\mathrm{a}}\omega_{\mathrm{t}})}$, $k_{\mathrm{p}} = \Phi_0^2/(2\mu_0\Lambda a^2)$ (provided $2\pi\Lambda \gg a$) is the spring constant given by the repulsive force with the lattice, see [47] and SI, and $\omega_{\mathrm{d}} = k_{\mathrm{p}}/\eta$ with η being the vortex viscosity coefficient, is the so-called depinning frequency, which marks the crossover between elastic motion, dominant at lower frequencies, and purely dissipative motion, arising at higher frequencies [48]. Using typical numbers for the vortex viscosity $\eta/\Lambda = 10^{-7}$ Kg/(s m) [48], these rates are remarkably small compared to the tunneling rate in Hubbard Hamiltonians, see Fig. 4. In the SI, we also estimate the damping rate in the harmonic motion of the atom due to the magnetic coupling to the overdamped vortex, which turns out to be negligible.

In the actual experiment there might be other sources of decoherence that we are not considering here. Practical considerations might also be very relevant. For instance, as analyzed in the SI, the position of the vortices has to be very accurate, with an error less than $1-2$ % in the distance between them. Otherwise, the trap depths and thereby the tunneling rates will fluctuate through the lattice. This can constitute a serious challenge in the nanofabrication of regular antidot lattices. In this respect, using triangular lattices spontaneously formed in a film without artificial pinning might be advantageous. The randomness in size and shapes of the antidots might also lead to imperfections, nevertheless, note that the flux in each vortex is given by the constant of nature Φ_0. Note that time dependent fields might induce dissipation in the vortices. As discussed before, we apply a time dependent field $\mathbf{B}_{\rm M}(t)$ to avoid Majorana losses. This field is parallel to the film, and in the ideal case, would not interact with the vortices. In any case, to reduce dissipation it will be convenient is to use $\omega_{\rm M} \ll \omega_{\rm d}$.

Magnetic local addressing

Finally, let us discuss the possibility to perform magnetic local addressing of the atoms in the lattice. We will use the fact thin films of $d \lesssim \lambda$ are effectively transparent to external magnetic fields, as explained below. Consequently, we propose to place a magnetic tip close to the bottom side of the film to locally interact with the atoms trapped above, see Fig. 5a. In the SI, we obtain the analytical expression of the magnetic field above the film for a given thickness d and London penetration depth λ. The ratio between the magnetic field $B^z_{\rm d}$ at $z = z_0 + d$ in the presence of a superconducting film with London penetration depth λ with the corresponding one in case of not having the film $B^z_{\rm d,0}$ depends on the dimensionless parameters λ/d and $L \equiv (z_0 + a_{\rm d})/d$, see SI. In Fig. 5b, this ratio is plotted as a function of λ/d for different L. Note that even for $\lambda = d$, $B^z_{\rm d} \sim B^z_{\rm d,0}/2$ for $L = 2$. As discussed in [50] the minimum distance for which the dipole will create a vortex is given by $a_1 = \Lambda\sqrt{\mu_0 m_{\rm d}/[\Phi_0 \Lambda \ln(\Lambda/\xi)]}$, this equation is valid for $a_1 > \Lambda$. With typical numbers (Λ = 100 nm and ξ = 10 nm), $a_1 \sim 2\Lambda$ for a dipole of magnetic moment $m_d \sim 10^8 \mu_{\rm B}$. Using the maximum magnetic moment and $\lambda = d = \Lambda = z_0 = a_{\rm d}/2 = 100$ nm (note that $L = 3$) this leads to a coupling to the atom of $g_{\rm d} \sim \mu_{\rm B} B^z_{\rm d}/\hbar \sim 0.4 \mu_{\rm B} B^z_{\rm d,0}/\hbar \sim 2\pi \times 10^8$ Hz. Since the neighbor atoms are farther away from the dipole, the coupling is reduced at least by a factor of two, which permits to perform local addressing by adding different phases into the internal state of the atoms. In order to measure the collective state of the atoms one can release them from the trap and perform time-of-flight measurements similarly to what is done in optical lattices [1]. Recall that the magnetic lattice can be switched off by decreasing the bias field B_1.

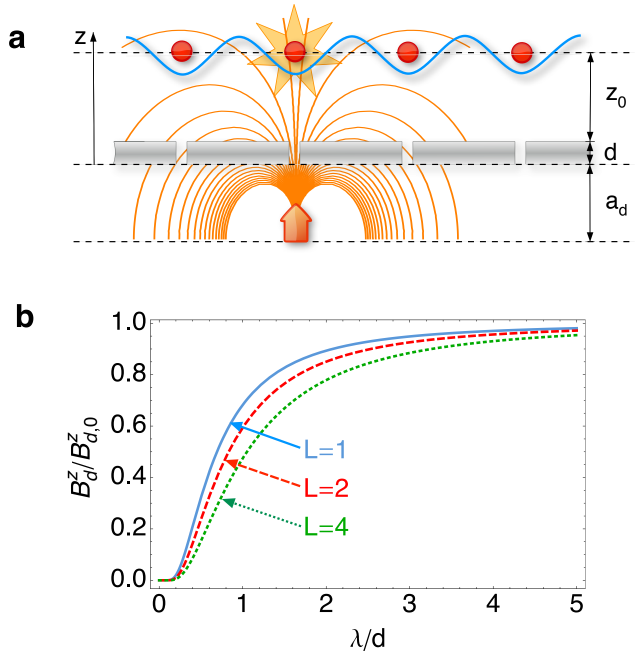

FIG. 5: **Magnetic local addressing.** a) An atom trapped at z_0 above a film of thickness d is magnetically addressed by approaching a magnetic tip at a distance $a_{\rm d}$ from below the film. b) The ratio between the field in the presence of the film over the same field without it $B^z_{\rm d}/B^z_{\rm d,0}$ is plotted as a function of λ/d for $L = (z_0 + a_{\rm d})/d = 1, 2, 4$. Note that we recover the expected limits: when $\lambda \ll d$ the superconductor completely shields the region above the film from the field of the dipole; when $\lambda \gg d$ the superconductor becomes almost transparent to the dipole field.

Outlook

To conclude, we have shown that the control and manipulation of superconducting vortices in thin films can be used to design a magnetic nanolattice for ultracold atoms. This is based on trapping neutral atoms near a surface in a superconducting state, whose macroscopic coherence leads to promising scalings regarding surface decoherence. In the quest of bringing quantum simulation into a non-classical regime, for instance, by simulating antiferromagnetism in Hubbard models and long-time quantum many-body dynamics, the SVL proposed here may provide a very useful path by boosting the energy-scales of the simulator by scaling down the lattice. The interplay between superconductivity and atomic physics, as proposed here, might pave the way towards all-magnetic schemes for quantum computation and simulation with neutral atoms as well as to side applications such as using cold atoms to probe important properties of high-T_c superconductivity.

Acknowledgements. We acknowledge funding from the EU projects AQUTE and ITN Coherence, Spanish Consolider NANOSELECT (CSD2007-00041) and MAT2012-35370 projects, and the Austrian Science Fund (FWF) through SFB FOQUS. We thank J. P. Ronzheimer for support with graphical illustrations.

Author contributions. ORI, PZ, and JIC proposed the original idea. ORI, CN and AS performed the calculations that were planned and discussed by all the authors. ORI drafted the manuscript and all the authors contributed to the final version.

Competing financial interests. The authors declare no competing financial interests.

[1] Bloch, I., Dalibard, J. & Zwerger, W. Many-body physics with ultracold gases. Rev. Mod. Phys. **80**, 885-964 (2008).

[2] Jaksch, D., Bruder C., Cirac J. I., Gardiner C. W.& Zoller, P. Cold bosonic atoms in optical lattices. Phys. Rev. Lett. **81**, 3108-3111 (1998).

[3] Bloch, I., Dalibard J. & Nascimbène. Quantum simulations with ultracold quantum gases. Nature Phys. **8**, 262-276 (2012).

[4] Lewenstein, M., Sanpera, A. & Ahufinger V. *Ultracold Atoms in Optical Lattices: Simulating quantum many-body systems.* (Oxford University Press, Oxford, 2012).

[5] Bloch, I. Quantum coherence and entanglement with ultracold atoms in optical lattices. Nature **453**, 1016-1022 (2008).

[6] Katori, H. Optical lattice clocks and quantum metrology. Nature Photon. **5**, 203210 (2011).

[7] Cirac, J. I. & Zoller P. Nature Phys. **8**, 264-266 (2012).

[8] Gullans, M., Tiecke, T., Chang, D. E., Feist, J., Thompson, J. D., Cirac, J. I., Zoller, P. & Lukin, M. D. Nanoplasmonic Lattices for Ultracold Atoms. Phys. Rev. Lett. **109**, 235309 (2012).

[9] Shimizu, F., Hufnagel, C. & Mukai T. Stable neutral atom trap with a thin superconducting disk. Phys. Rev. Lett. **103**, 253002 (2009).

[10] Müller, T., Zhang, B., Fermani R., Chan, K. S., Lim, M. J. & Dumke R. Programmable trap geometries with superconducting atom chips. Phys. Rev. A **81**, 053624 (2010).

[11] Müller, T., Zhang, B., Fermani R., Chan, K. S., Wang, Z. W., Zhang, C. B., Lim, M. J. & Dumke R. Trapping of ultra-cold atoms with the magnetic field of vortices in a thin-film superconducting micro-structure. New J. Phys. **12**, 043016 (2010).

[12] Zhang, B., Siercke, M., Chan, K. S., Beian, M., Lim, M. J. & Dumke R. Magnetic confinement of neutral atoms based on patterned vortex distributions in superconducting disks and rings. Phys. Rev. A **85**, 013404 (2012).

[13] Siercke, M., Chan, K. S., Zhang, B., Beian, M., Lim, M. J. & Dumke R. Reconfigurable self-sufficient traps for ultracold atoms based on a superconducting square. Phys. Rev. A **85**, 041403(R) (2012).

[14] Markowsky, A., Zare, A., Graber, V. & Dahm T. Optimal thickness of rectangular superconducting microtraps for cold atomic gases. Phys. Rev. A **86**, 023412 (2012).

[15] Moshchalkov, V., Woerdenweber, R. & Lang, W. *Nanoscience and Engineering in Superconductivity* Ch. 2 (Springer-Verlag, Berlin Heidelberg, 2010).

[16] Grabowski A. & Pfau, T. A lattice of magneto-optical and magnetic traps for cold atoms. Eur. Phys. J. D **22**, 347-354 (2003).

[17] Singh, M., Volk, M., Akulshin, A., Sidorov, A., McLean, R. & Hannaford, P. One-dimensional lattice of permanent magnetic microtraps for ultracold atoms on an atomic chip. J. Phys. B: At. Mol. Opt. Phys. **41**, 065301 (2008).

[18] Whitlock, S., Gerritsma, R., Fernholz, T. & Spreeuw, R. J. C. Two-dimensional array of microtraps with atomic shift register on a chip. New J. Phys. **11**, 023021 (2009).

[19] Abdelrahman, A., Vasiliev, M., Almeh, K. & Hannaford P. Asymmetrical two-dimensional magnetic lattices for ultracold atoms. Phys. Rev. A **82**, 012320 (2010).

[20] de Gennes, P. G. *Superconductivity of metals and alloys.* (Westview Press, Boulder, 1999).

[21] Buzdin, A. & Feinberg, D. Electromagnetic pinning of vortices by non-superconducting defects and their influence on screening. Physica C **256**, 303 (1996).

[22] Nordborg, H. & Vinokur,V. M. Interaction between a vortex and a columnar defect in the London approximation. Phys. Rev. B **62**, 12408 (2000).

[23] Brandt, E. H. Ginzburg-Landau vortex lattice in superconductor films of finite thickness. Phys. Rev. B **71**, 014521 (2005).

[24] Pearl, J. Current distribution in superconducting films carrying quantized fluxoids. Appl. Phys. Lett. **5**, 65 (1964).

[25] Clem, J. R. Two-dimensional vortices in a stack of thin superconducting films: A model for high-temperature superconducting multilayers. Phys. Rev. B **43**, 7837 (1991).

[26] Carneiro, G. & Brandt, E. H. Vortex lines in films: fields and interactions. Phys. Rev. B **61**, 6370-6376 (2000).

[27] Pogosov, W. V., Rakhmanov, A. L. & Moshchalkov, V. V. Vortex lattice in the presence of a tunable periodic pinning potential. Phys. Rev. B **67**, 014532 (2003).

[28] Folman, R., Krüger, P., Schmiedmayer, J., Denschlag, J. & Henkel C. Microscopic atom optics: from wires to an atom chip. Adv. in At. Mol. Opt. Physics **48**, 263-356 (2002).

[29] Fortágh, J. & Zimmermann C. Magnetic microtraps for ultracold atoms. Rev. Mod. Phys. **79**, 235-289 (2007).

[30] Sanchez, A. & Navau, C. Magnetic properties of finite superconducting cylinders. I. Uniform applied field. Phys. Rev. B **64**, 214506 (2001).

[31] Chen, D.-X., Navau C., Del-Valle, N. & Sanchez, A. Effective penetration depths of a thin type-II superconducting strip. Supercond. Sci. Technol. **21**, 105010 (2008).

[32] Brandt, E. H. Thin superconductors and SQUIDs in perpendicular magnetic field. Phys. Rev. B **72**, 024529 (2005).

[33] Brink, D. M. & Sukumar, C. V. Majorana spin-flip transitions in a magnetic trap. Phys. Rev. A **74**, 035401 (2006).

[34] Petrich, W., Anderson, M. H., Ensher, J. R. & Cornell, E. A. Stable, Tightly Confining Magnetic Trap for Evaporative Cooling of Neutral Atoms. Phys. Rev. Lett. **74**, 3352 (1995).

[35] Hofstetter, W., Cirac J. I., Zoller P., Demler E. & Lukin M. D. High-temperature superfluidity of fermionic atoms in optical lattices. Phys. Rev. Lett. **89**, 220407 (2002).

[36] Greif, D., Uehlinger, T., Jotzu, G., Tarruell, L. & Esslinger T. Quantum magnetism of ultracold fermions in an optical lattice. arXiv:1212.2634.

[37] Lee, P., Nagosa, N. & Wen, X.-G. Doping a Mott insulator: Physics of high-temperature superconductivity. Rev. Mod. Phys. **78**, 17-85 (2006).

[38] Henkel, C., Pötting, S. & Wilkens, M. Loss and heating of particles in small and noisy traps. Appl. Phys. B. **69**, 379-387 (1999).

[39] Henkel, C., Krüger, P., Folman, R. & Scmiedmayer J. Fundamental limits for coherent manipulation on atom chips. Appl. Phys. B. **76**, 173-182 (2003).

[40] Skagerstam, B.-S. K., Hohenester, U., Eiguren, A. & Rekdal P. K. Spin decoherence in superconducting atom chips. Phys. Rev. Lett. **97**, 070401 (2006).

[41] Hohenester, U., Eiguren, A., Scheel, S. & Hinds, E. A. Spin-flip lifetimes in superconducting atom chips: Bardeen-Cooper-Schrieffer versus Eliashberg theory. Phys. Rev. A **76**, 033618 (2007).

[42] Skagerstam, B.-S. & Rekdal, P. K. Photon emission near superconducting bodies. Phys. Rev. A **76**, 052901 (2007).

[43] Hufnagel, C., Mukai, T. & Shimizu, F. Stability of a superconductive atom chip with persistent current. Phys. Rev. A **79**, 053641 (2009).

[44] Kasch, B., Hattermann, H., Cano, D., Judd, T. E., Scheel, S., Zimmermann, C., Kleiner, R., Koelle, D. & Fortágh, J. Cold atoms near superconductors: atomic spin coherence beyond the Johnson noise limit. New J. Phys. **12**, 065024 (2010).

[45] Nogues G. *et al.*. Effect of vortices on the spin-flip lifetime of atoms in superconducting atom-chips. Europhys. Lett. **87**, 13002 (2009).

[46] Fruchtman, A. & Horovitz B. Single vortex fluctuations in a superconducting chip as generating dephasing and spin flips in cold atom traps. Europhys. Lett. **99**, 53002 (2012).

[47] Brandt, E. H. Vortex-vortex interaction in thin superconducting films. Phys. Rev. B **79**, 134526 (2009).

[48] Pompeo, N. & Silva, E. Reliable determination of vortex parameters from measurements of the microwave complex resistivity. Phys. Rev. B **78**, 094503 (2008).

[49] Golubchik, D., Polturak, E. & Koren, G. Mass of a vortex in a superconducting film measured via magneto-optical imaging plus ultrafast heating and cooling. Phys. Rev. B **85**, 060504(R) (2012).

[50] Wei, J. C., Chen, J. L., Horng, L. & Yang, T. J. Magnetic force acting on a magnetic dipole over a superconducting thin film. Phys. Rev. B **54**, 15429 (1996).